IEEE Transactions on Sustainable Energy, Volume 11, Issue 4, October 2020, pp. 2567 - 2580
DOI:10.1109/TSTE.2020.2966737

A Fixed-point Based Distributed Method for Energy Flow Calculation in Multi-Energy Systems

Gang Zhang, *Student Member*, *IEEE*, Feng Zhang, *Member*, *IEEE*, Ke Meng, *Member*, *IEEE*, Xin Zhang, *Member*, *IEEE*, and Zhao Yang Dong, *Fellow*, *IEEE*

***Abstract*— Energy flow calculation (EFC) plays an important role in steady-state analysis of multi-energy systems (MESs). However, the independent management of sub-energy systems (subsystems) poses a considerable challenge to solve the high-order nonlinear energy flow model due to the limited information exchange between these subsystems. In this paper, a fixed-point based distributed method is proposed for EFC in an electricity-gas-heating system. Firstly, the mathematical modeling of each subsystem with coupling units is introduced. Then, two information exchange structures among subsystems are presented as sequential and parallel structures. Based on the fixed-point theorem, novel distributed sequential and parallel methods for EFC are proposed to calculate energy flow distribution in MESs. In our proposed method, the EFC in subsystems is implemented by the individual system operators, with limited information exchange between subsystems. Therefore, the information privacy of subsystems can be preserved in this solution process. Moreover, the convergence of the proposed method is guaranteed, and the sufficient conditions for the convergence are presented. Lastly, simulations on a MES demonstrate the effectiveness of the proposed method and the quantified superiority over the existing methods in computation time, accuracy and reliability.**

***Index Terms*—Distributed method, energy flow calculation, fixed-point, high-order nonlinear equation, multi-energy system.**

NOMENCLATURE

1) Variables and Parameters in Electricity Systems

B_{ij} , G_{ij}	Susceptance and conductance of line ij.
N_e	Total number of electrical buses.
N_e^1, N_e^2, N_e^3	Number of slack node, PQ node and PV node.
N_e^{total}	Total number of electrical equations.
P_i^g, Q_i^g	The injected active and reactive power at bus i.
P^{ge}	The power generated by the units except for those at electrical and heating slack nodes.
P_i^l, Q_i^l	The active and reactive loads at bus i.
P^{loss}	The power loss of whole networks.
ΔP_i , ΔQ_i	Active and reactive power mismatches at bus i.
P^{le}	The general electric load.
$\|V_i\|$, θ_i	Voltage magnitude and angle at bus i and j.
θ_{ij}	Voltage angle difference between bus i and j.

2) Variables and Parameters in Natural Gas Systems

C_{mn}	The pipeline constant.
f_{in}	The gas flow pressurized by the compressor.
f_{mn}^{comp}	The gas flow consumed by the compressor mn;
f_m^l	Gas flow consumed by the gas load at node m.
f_{mn}^p	Gas flow through pipeline mn.
f_m^s	Gas flow extracted from gas sources at node m.
Δf_m	The mismatch of nodal gas flow at node m.
N_g	Total number of gas nodes.
P_{mn}^{comp}	The active power consumed by compressor mn;
N_g^{total}	Total number of gas equations.
N_g^1, N_g^2	Number of slack node and known-injection node.
α	The polytropic exponent.
γ_{mn}^{comp1} , γ_{mn}^{comp2} , γ_{mn}^{comp3}	Consumption coefficients of compressor mn.
η_{mn}^{comp}	The compressor efficiency.
ρ_{in}, ρ_o	Inlet and outlet pressures of the compressor.
ρ_m	The gas pressures at nodes m.

3) Variables and Parameters in Heating Systems

c_p	The specific heat of water.
L_{ab}	The length of pipeline ab.
m_{ab}	Mass flow from node a to b.
m_a^l m_a^s	Mass flow of heating load and source at node a.
m_a^p	The water mass to be pressured by the pump a.
Δm_a	The mismatch of water mass at node a.
N_h	Total number of heating nodes.
N_h^1, N_h^2 , N_h^3	The number of slack node, ϕT^s node and ϕT^r node.
N_h^l, N_h^{loop} , N_h^s	Number of demand nodes, loops and source nodes.
N_h^{st}	The number of heating sources at one node.
N_h^{total}	Total number of heating equations.
P_a^p	The electrical power of pump a.
pr_a^p	The water pressure at node a.
Δp_{ab}	The pressure losses in pipeline ab.
Δp_k^l	The pressure mismatch of the k^{th} loop.
T_g	The ambient temperature.
T_a^s , T_a^r	The supply and return temperatures
$T_a^{s,s}$	The supply temperature of heat sources at node a.
$T_a^{r,l}$	The return temperature of heating load at node a.
ΔT_a^s , ΔT_a^r	The mismatches of supply and return temperature at node a.
U	The heat transfer coefficient per unit length.

G. Zhang and F. Zhang are with the Key Laboratory of Power System Intelligent Dispatch and Control, Ministry of Education, Shandong University, Jinan, 250061, China (e-mail: fengzhang@sdu.edu.cn).

K. Meng and Z. Y. Dong are with the School of Electrical Engineering and Telecommunications, The University of New South Wales, NSW 2052, Australia (e-mail: kemeng@ieee.org, zydong@ieee.org).

X. Zhang is with the Energy and Power Theme, School of Water, Energy and Environment, Cranfield University, Cranfield MK43 0AL, U.K. (e-mail:, xin.sam.zhang@gmail.com).

ϕ_a^l , ϕ_a^s	Heating power of demand and source at node *a*.
$\Delta\phi_a^l$, $\Delta\phi_a^s$	The mismatch of heating power of source and demand at node *a.*
η_a^p	The efficiency of the pump at node *a*.
ρ^w	The water density.

4) Variables and Parameters Related to Coupling Units

a_i^C , b_i^C , d_i^C , L_i^1 , L_i^2 , r_i^1 , r_i^2	Coefficients of the CHP model;
f_i^C , f_a^B, f_i^G	The gas flows consumed by the CHP at bus *i*, GB at node *a* and GT at bus *i*.
P_i^C , P_i^G	The active power of the CHP and GT at bus *i*.
P^{le}	The general electric load
q_{gas}	The heat value of natural gas
T_i^C	The supplied temperature of the CHP at bus *i*.
$\gamma_a^{B_1}$, $\gamma_a^{B_2}$, $\gamma_a^{B_3}$	The consumption coefficients of the GB at node *a*.
$\gamma_i^{G_1}$, $\gamma_i^{G_2}$, $\gamma_i^{G_3}$	The consumption coefficients of GT at bus *i*.
ϕ_a^B ,ϕ_i^C	Heating power of GB at node *a* and CHP at bus *i*.
ϕ_i^{min} , ϕ_i^{max}	The minimum and rated heating power of the CHP at bus *i*.
η_i^C	The efficiency of CHP at bus *i.*
μ	The spectral radius.

5) Additional Unknown Variables

f_{hs}^B , f_{hs}^C	Gas flow consumed by the GB and CHP at heating slack node *hs*.
f_{es}^C , f_{es}^G,	Gas flow consumed by the CHP and GT at electrical slack node *es*.
P_{es}^C, P_{es}^G	Active power of the CHP and GT at electrical slack node *es*.
P_{hs}^C	Active power of the CHP at heating slack node *hs*.
P^{comp}	The active power consumed by compressors.
P^p	The electrical power of pumps.
ϕ_{es}^C	Heating power of CHP at electrical slack node *es*.
ϕ_{hs}^B, ϕ_{hs}^C	Heating power of the GB and CHP at heating slack node *hs*.

6) Acronyms

CHP	Combined heat and power plant.
EFC	Energy flow calculation.
EH	Energy hub.
ESO	Electricity system operator.
FPDPM	Fixed-point based distributed parallel method.
FPDSM	Fixed-point based distributed sequential method.
GB	Gas boiler.
GSO	Gas system operator.
GT	Gas turbines.
HSO	Heating system operator.
IH	Information hub.
MES	Multi-energy system.
UNM	Unified Newton-Raphson method.

I. Introduction

MULTI-ENERGY systems (MESs) were initially proposed to link independent sub-energy systems (subsystems) together as a whole energy system to improve techno-economic and environmental performance, which is considered as an effective solution to tackle climate change and energy crisis [1]-[3]. The interaction and interdependency of MESs are strengthened by the increasing penetration of cogeneration systems, such as combined heat and power plants (CHPs) with high energy conversion efficiency [4]-[6]. To achieve optimal planning and operation of a MES, the coordinated analysis of multi-energy carriers is desirable [7]-[8].

As a basic tool, energy flow calculation (EFC) plays a significant role in steady-state analysis of MESs, such as day-ahead dispatch [9], static security analysis [10] and service restoration [11]. However, high-order nonlinear EFC models are challenging to solve due to the limited information sharing between subsystems, which are generally managed by different operators.

Studies have been conducted to solve EFC models in an individual electricity, gas or heating system, such as Newton's method and holomorphic embedding (HE) for electrical power flow calculation[12]-[14], Newton's method for gas flow calculation[15], and graph theory method for heating flow calculation [16]-[17]. However, these EFC methods for individual energy systems cannot be directly employed in subsystems of MES, because of additional unknown variables from other subsystems that lead to the EFC non-executable. For example, electric load related information is well given in the traditional electricity system for solving EFC problem. However, in MES, the electrical power consumption of compressors is determined by gas flow distribution, which is treated as an unknown load variable of EFC in electrical subsystem. Hence, the implementation of EFC in electrical subsystem relies on the gas subsystem, and the previous methods for electrical EFC are no longer effective. Consequently, the interdependence between electricity, gas and heating subsystems of MES should be comprehensively studied, and an efficient method is required to solve the EFC in MES.

Based on the interaction mechanism between subsystems, the unified Newton-Raphson method (UNM) has been customized for the EFC in electricity-gas systems [18], electricity-heating system [19] and electricity-gas-heating systems [20]-[22]. In UNM, all EFC equations related to subsystems are simultaneously solved in a central place, so that the information of whole MES need to be shared and aggregated by a joint operator [23]. However, this approach is normally impractical, because electricity, gas and heating systems are generally managed by different entities. Due to the risk aversion and technical limitation of data management, subsystem operators tend to preserve the information privacy rather than collaborative data sharing [24]. Furthermore, without a robust and digitalized energy system, intensively sharing large amounts of information in the UNM brings the increased communication burden, and the information sharing scheme threatens the robustness of the UNM solution under the situation of possible data loss and incomplete dataset. In addition, a large number of variables in a MES will significantly increase the dimension of Jacobian matrix in the UNM, which will generally lead to slow or non- convergence. Consequently, it is necessary to develop a distributed and decentralized method for the joint EFC in MESs because 1) computationally, the dimension of the distributed

This article has been accepted for publication in a future issue of this journal, but has not been fully edited. Content may change prior to final publication. Citation information: DOI 10.1109/TSTE.2020.2966737, IEEE Transactions on Sustainable Energy

method is significantly decreased by decomposing the EFC of MESs into several sub-EFCs in the respective subsystems; 2) effective solution methods for EFC in subsystems, such as HE, can be utilized to accelerate the EFC process; and 3) the distributed method can preserve the autonomy of subsystems and enhance robustness against data loss.

The structure of information exchange among subsystems is vital to develop the distributed method for the EFC in MESs, which determines information flow in the solution process. Two different information exchange structures in MESs can be implemented in practice, denoted as ***Structures (a)*** and ***(b)*** [23]. In ***Structure (a)***, the information flows as a loop in a sequential way across the electricity system operator (ESO), gas system operator (GSO) and heating system operator (HSO). In ***Structure (b)***, the information flows under a radial structure, i.e., ESO, GSO and HSO can simultaneously exchange certain information through the information hub (IH) at the root bus. However, the existing solution methods for EFC are non-compatible with both 'loop' and 'radial' structures.

To enable the compatible solution that could adapt to various information exchange structures across the subsystems, a fixed-point based distributed method is proposed in this paper. The contributions of this paper are summarized as follows:

1) According to ***Structure (a)***, a novel fixed-point based distributed sequential method (FPDSM) is presented. In this case, subsystem operators have independent control over individual subsystems, and the overall EFC can be carried out in a distributed sequential way based on the loop information flow.

2) According to ***Structure (b)***, a novel fixed-point based distributed parallel method (FPDPM) is proposed. In the FPDPM, certain information is exchanged between an IH and subsystem operators. Specifically, the IH processes the information from subsystems and exchanges the information to subsystem operators. Then, subsystem operators can carry out their EFCs in parallel.

3) The proposed method can converge to the fixed point in finite iterations. Moreover, simulations on a MES demonstrate that the FPDSM and FPDPM have improved performance over existing methods in computation time, accuracy and robustness against data loss.

This paper is organized as follows. The schematic overview of the modeling methodology is shown in Section II. The MES is modeled in Section III. The distributed method for the EFC is proposed in Section IV. Simulation results are calculated in Section V. Finally, our conclusion is drawn in Section VI.

II. Overview of the Modeling Methodology

In this section, the structure of the modeling methods is summarized. As shown in Fig.1, the MES is modeled as electricity, gas and heating subsystems with coupling units in Section III. Then, the distributed EFC method is proposed to solve the MES model in Section IV. Specifically, the additional unknown variables in EFC of subsystems are presented in Section IV-A, and then the loop and radial structures of information exchange among subsystems are designed in Section IV-B. According to the two different structures of information exchange, fixed-point based EFC methods are proposed respectively in Section IV-C, including FPDSM and FPDPM. Subsequently, conditions and supplements of the distributed EFC method are presented, including sufficient conditions for convergence in Section IV-D, initial value estimation for unknown variables in Section IV-E, superiority of the proposed method over the independent EFC method and the UNM method in Section IV-F, and discussions of model adaptability to other coupling networks and the application scope in Section IV-G. Lastly, the effectiveness of the proposed method is demonstrated, and the superiority over other existing method is validated by numerical tests in Section V.

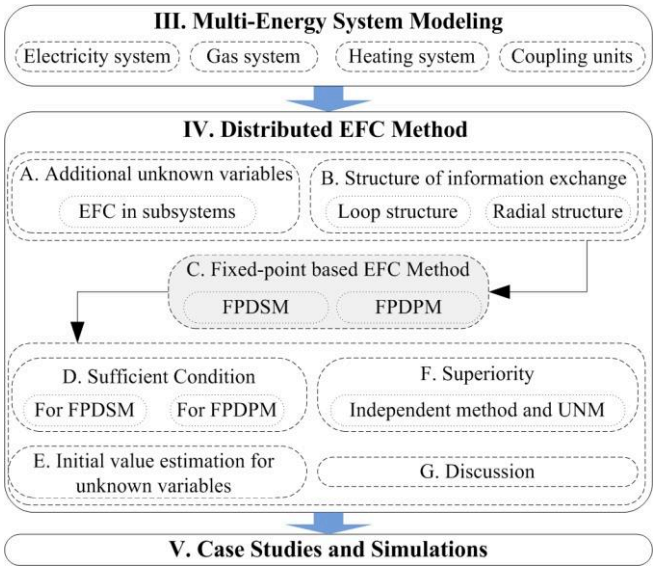

Fig. 1. Schematic overview of the modeling methodology

III. Multi-Energy System Modeling

In this section, a MES consists of electricity, gas, and heating subsystems as well as various coupling units, such as combined heat and power (CHPs), gas boilers (GBs) and gas turbines (GTs), are comprehensively modeled.

A. Electricity System

The modeling of electricity system consists of active and reactive power nodal balance equations [25]-[26], as shown in (1) and (2), respectively. In the classic electricity model, there are total number of $N_e^{total}=2\cdot N_e^2+N_e^3$ equations corresponding to $(2\cdot N_e^2+N_e^3)$ unknown variables, i.e., voltage magnitudes and angles with the number of N_e^2 and $N_e^2+N_e^3$, respectively.

$$\Delta P_i=P_i^g-P_i^l-\sum_{j=1}^{N_e}|V_i||V_j|\left(G_{ij}\cos\theta_{ij}+B_{ij}\sin\theta_{ij}\right),\ \forall i=1,2,\cdots,N_e^2+N_e^3 \quad (1)$$

$$\Delta Q_i=Q_i^g-Q_i^l-\sum_{j=1}^{N_e}|V_i||V_j|\left(G_{ij}\sin\theta_{ij}-B_{ij}\cos\theta_{ij}\right),\ \forall i=1,2,\cdots,N_e^2 \quad (2)$$

B. Gas System

The modeling of natural gas system contains nodal gas flow balance equations (3) [20], which are built for all known-injection nodes. Consequently, there are total number of $N_g^{total}=N_g^2$ equations corresponding to N_g^2 pressure variables.

This article has been accepted for publication in a future issue of this journal, but has not been fully edited. Content may change prior to final publication. Citation information: DOI 10.1109/TSTE.2020.2966737, IEEE Transactions on Sustainable Energy

$$\Delta f_m = f_m^s - f_m^l + \sum_{n=1}^{N_g} f_{mn}^p = 0, \quad \forall m = 1,2,\cdots,N_g^2 \tag{3}$$

In addition, the gas flow equation for general pipelines (4), and the power and gas consumption model of compressors (5-6) are shown as supplementary equations to Eq. (3) [20]. It is noted that sign(ρ_m, ρ_n) in (4) denotes the direction of the gas flow in pipeline *mn*. For example, sign(ρ_m, ρ_n) =1 represents $\rho_m > \rho_n$, and gas flows from node *m* to node *n*.

$$f_{mn}^p = C_{mn}\text{sign}(\rho_m,\rho_n)\cdot\left[\text{sign}(\rho_m,\rho_n)\cdot\left(\rho_m^2-\rho_n^2\right)\right]^{0.5} \tag{4}$$

$$P_{mn}^{comp} = \frac{f_{in}\alpha}{\eta_{mn}^{comp}(\alpha-1)}\left[\left(\rho_o/\rho_{in}\right)^{(\alpha-1)/\alpha}-1\right] \tag{5}$$

$$f_{mn}^{comp} = \gamma_{mn}^{comp_1} + \gamma_{mn}^{comp_2} P_{mn}^{comp} + \gamma_{mn}^{comp_3}\left(P_{mn}^{comp}\right)^2 \tag{6}$$

C. Heating System

The heating system model comprises of the nodal supply and return temperature differences (7)-(8), nodal heating power demand equation (9), nodal heating power source equation (10), nodal water mass balance equation (11) and head loss equation (12) [16]. It is noted that $\text{sign}_1(m_{ba})$ in (11) is the sign function, where $\text{sign}_1(m_{ba})$ =1 when m_{ba} >0, and otherwise $\text{sign}_1(m_{ba})$=0; and $\text{sign}_2(m_{ab})$ in (12) is a sign function with a value of +1 if m_{ab} is in the *k* loop and its direction is same as the predefined loop direction, −1 if opposite, and 0 if *ab* is not in the loop.

$$\Delta T_a^s = T_a^s\cdot\left[m_a^l + \sum_{b=1}^{N_h}\text{sign}_1(m_{ab})\cdot m_{ab}\right] - m_a^s T_a^{s,s} - \sum_{b=1}^{N_h}\text{sign}_1(m_{ba}) \cdot m_{ba}\cdot\left[\left(T_b^s - T_g\right)\exp\left(-\frac{UL_{ab}}{c_p m_{ba}}\right)+T_g\right], \quad \forall a = 1,2,\cdots,N_h \tag{7}$$

$$\Delta T_a^r = T_a^r\cdot\left[m_a^s + \sum_{b=1}^{N_h}\text{sign}_1(m_{ba})\cdot m_{ba}\right] - m_a^l T_a^{r,l} - \sum_{b=1}^{N_h}\text{sign}_1(m_{ab}) \cdot m_{ab}\cdot\left[\left(T_b^r - T_g\right)\exp\left(-\frac{UL_{ab}}{c_p m_{ab}}\right)+T_g\right], \quad \forall a = 1,2,\cdots,N_h \tag{8}$$

$$\Delta\phi_a^l = \phi_a^l - m_a^l c_p\left(T_a^s - T_a^{r,l}\right), \quad \forall a = 1,2,\cdots,N_h^l \tag{9}$$

$$\Delta\phi_a^s = \phi_a^s - m_a^s c_p\left(T_a^{s,s} - T_a^r\right), \quad \forall a = 1,2,\cdots,N_h^s \tag{10}$$

$$\Delta m_a = m_a^s - m_a^l + \sum_{b=1}^{N_h}\left[\text{sign}_1(m_{ba})\cdot m_{ba} - \text{sign}_1(m_{ab})\cdot m_{ab}\right], \forall a = 1,2,\cdots,N_h \tag{11}$$

$$\Delta p_k^l = \sum_{a=1}^{N_h}\sum_{b=1}^{N_h}\text{sign}_2(m_{ab})\cdot\Delta p_{ab}, \forall k = 1,2,\cdots,N_h^{loop} \tag{12}$$

Furthermore, if the number of heating sources at node *a* is N_h^{st}, the number of equations derived from Eq. (10) is $N_h^{st}\times N_h^s$, and the total number of equations is $N_h^{total} = 3N_h + N_h^l + N_h^{st}\times N_h^s + N_h^{loop}$. Correspondingly, the number of unknown variables is $3N_h + N_h^l + N_h^{st}\times N_h^s + N_h^{loop}$, i.e., T_a^s, T_a^r, m_a^l, m_a^s, m_{ab} and the heating power of CHP or GB at the heating slack node, with the number of N_h, N_h, N_h^l, $N_h^{st}\times N_h^s$, $N_h + N_h^{loop} - 1$ and 1, respectively.

The power consumption of pumps P_a^p is modeled by Eq. (13).

$$P_a^p = \left(pr_a^p\cdot m_a^p/\rho^w/\eta_a^p\right)\times 10^{-6} \tag{13}$$

D. Coupling Units

The coupling units contain CHPs, GTs, GBs, electric pumps and compressors. In addition to the models of electric compressors and pumps in Eqs. (5)-(6) and (13), an three line model of CHPs is adopted in this paper, which takes into account the changes of the power production at part load operation [27], details are shown in (14)-(17). Moreover, models of GBs in Eq. (18) and GTs in Eq. (19) are introduced, and these models have been widely employed in the EFC of MESs [17], [20].

$$P_i^C = \begin{cases} a_i^C\phi_i^C + b_i^C T_i^C + d_i^C, & L_i^1\phi_i^{\max} \le \phi_i^C \le \phi_i^{\max} \\ a_i^C\phi_i^C + b_i^C T_i^C + d_i^C - w_i^1, & L_i^2\phi_i^{\max} \le \phi_i^C \le L_i^1\phi_i^{\max} \\ a_i^C\phi_i^C + b_i^C T_i^C + d_i^C - w_i^1 - w_i^2, & \phi_i^{\min} \le \phi_i^C \le L_i^2\phi_i^{\max} \end{cases} \tag{14}$$

$$w_i^1 = \left(L_i^1\phi_i^{\max} - \phi_i^C\right)\cdot r_i^1 \tag{15}$$

$$w_i^2 = \left(L_i^2\phi_i^{\max} - \phi_i^C\right)\cdot r_i^2 \tag{16}$$

$$f_i^C = \left(P_i^C + \phi_i^C\right)/\left(q_{\text{gas}}\eta_i^C\right) \tag{17}$$

$$f_a^B = \gamma_a^{B_1} + \gamma_a^{B_2}\phi_a^B + \gamma_a^{B_3}\left(\phi_a^B\right)^2 \tag{18}$$

$$f_i^G = \gamma_i^{G_1} + \gamma_i^{G_2} P_i^G + \gamma_i^{G_3}\left(P_i^G\right)^2 \tag{19}$$

An energy hub (EH) is adopted in this paper to manage coupling units [28], and a typical EH model is shown in Fig. 2. Briefly, the CHP consumes gas from gas networks and generates electrical and heating power, and GB and GT consume gas to generate heating and electrical power, respectively.

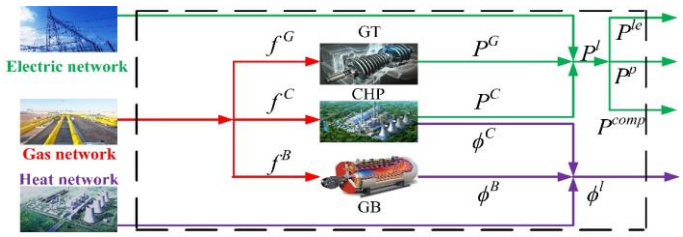

Fig. 2. A typical EH model

IV. Distributed EFC Method

A novel fixed point distributed method for EFC in MESs is presented in this section. Firstly, additional unknown variables incurred by interconnection of multi-energy subsystems are presented. Then, two structures of information exchange are proposed. Lastly, the distributed EFC methods are proposed, and the sufficient condition for convergence is derived.

A. Additional Unknown Variables

When the EFCs of individual subsystems are interconnected in MESs, additional unknown variables appear through the coupling units as described in Table I, where *hs* and *es* denote the heating slack node and electrical slack node, respectively. Additional unknown variables may cause EFC non-executable in a given subsystem if certain key variables are unknown. For example, the EFC in electricity subsystem cannot be conducted without the special electric load P^{comp}, which is determined by gas systems. This indicates that EFC in electricity system relies on the gas flow distribution. The key variables that impact EFC across subsystems are identified in Table I.

This article has been accepted for publication in a future issue of this journal, but has not been fully edited. Content may change prior to final publication. Citation information: DOI 10.1109/TSTE.2020.2966737, IEEE Transactions on Sustainable Energy

TABLE I ADDITIONAL UNKNOWN VARIABLES UNDER THE MES

System types	Additional unknown variables	Coupled systems
Electricity system	P^{comp}	Gas system
	P^{p}, P^{C}_{hs}	Heating system
Heating system	ϕ^{C}_{es}	Electricity system
Gas system	f^{C}_{hs}, f^{B}_{hs}	Heating system
	f^{G}_{es}, f^{C}_{es}	Electricity system

B. Structures of Information Exchange

To enable the convergence of EFCs in MES, the information exchange through subsystems plays an important role in designing the distributed methods. Generally, there are two structures of information exchange, which can be implemented in practice. In ***Structure (a)***, as shown in Fig. 3-a, the information related to additional unknown variables flows among subsystem with a peer-to-peer structure, so a loop diagram can be formed. In ***Structure (b)***, as shown in Fig. 3-b, the information regarding additional unknown variables from the ESO, GSO and HSO, i.e., (P^{comp}, P^{C}_{es}, P^{G}_{es}, P^{p}, ϕ^{C}_{hs}, ϕ^{B}_{h}), have been aggregated by an information hub (IH) at the root bus. In this radial structure, (P^{comp}, P^{C}_{es}, P^{G}_{es}, P^{p}, ϕ^{C}_{hs}, ϕ^{B}_{h}) are further translated to (f^{C}_{hs},f^{B}_{hs},f^{C}_{es},f^{G}_{es}) for the GSO, (P^{C}_{hs}, P^{p}, P^{comp}) for the ESO and (ϕ^{C}_{es}) for the HSO. Finally, the processed variables are distributed to the GSO, ESO and HSO, so a radial diagram is developed.

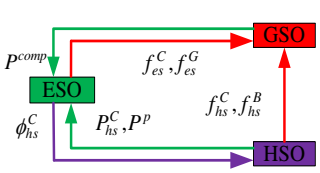

Fig. 3-a. The loop diagram of information exchange in ***Structure (a)***

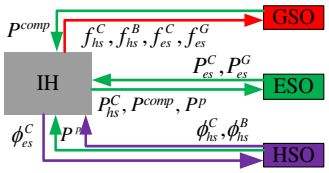

Fig. 3-b. The radial diagram of information exchange in ***Structure (b)***

C. The Fixed-Point Based Distributed Method

Based on the two structures of information exchange, the corresponding FPDSM and FPDPM are proposed in this section. As an example, the most comprehensive coupling relationship among subsystems is chosen for the proposed method. In this coupling structure, the electrical and heating slack nodes are both powered by the CHPs which simultaneously couple the electrical, gas and heating systems. In general, the proposed method can be adapted to other coupling relationships, which will be discussed in Section IV-G.

For simplicity, the EFC models of subsystems are described in compact form, as shown in Eqs. (20), where $\mathrm{F}_e(\cdot)$, $\mathrm{F}_g(\cdot)$ and $\mathrm{F}_h(\cdot)$ are the electrical EFC model (1)-(2), gas EFC model (3)-(6) and heating EFC model (7)-(13), respectively; $[\cdot]_e$, $[\cdot]_g$, $[\cdot]_h$ are variable sets that can be obtained by conducting EFC in the electrical, gas and heating systems, respectively; and $(\cdot)$ denotes sets of additional unknown variable that need to be pre-determined by other system operators.

$$\begin{cases} [P^{C}_{es}]_e=\arg\{\mathrm{F}_e\left(P^{comp},P^{p},P^{C}_{hs}\right)=0\} \\ [P^{p},\phi^{C}_{hs}]_h=\arg\{\mathrm{F}_h\left(\phi^{C}_{es}\right)=0\} \\ [P^{comp}]_g=\arg\{\mathrm{F}_g\left(f^{C}_{hs},f^{C}_{es}\right)=0\} \end{cases} \tag{20}$$

In ***Structure (a)***, the subsystem operators exchange information in a peer-to-peer way. Consequently, a novel FPDSM is developed where the EFC in heating, gas and electrical subsystems are sequentially implemented. The detailed FPDSM and information flow are shown in Algorithm 1 and Figure 4-a, which match the loop diagram in Fig. 3-a.

Algorithm 1: The FPDSM based on *Structure (a)*.

1: ***Initialization.*** Define tolerance ε, the indices of iterations k=0; pre-estimate the initial value of P^{C}_{es}, termed as $P^{C(0)}_{es}$.

2: ***EH at electrical slack node.*** Solve Eq. (21), and obtain $f^{C(k)}_{es}$ and $\phi^{C(k)}_{es}$. Pass $\phi^{C(k)}_{es}$ and $f^{C(k)}_{es}$ to HSO and GSO, respectively.

$$\begin{cases} P^{C(k)}_{es}=\begin{cases} a^{C}_{es}\phi^{C(k)}_{es}+b^{C}_{es}T^{C}_{es}+d^{C}_{es}, & L^{1}_{es}\phi^{\max}_{es}\le\phi^{C}_{es}\le\phi^{\max}_{es} \\ a^{C}_{es}\phi^{C(k)}_{es}+b^{C}_{es}T^{C}_{es}+d^{C}_{es}-w^{1}_{es}, & L^{2}_{es}\phi^{\max}_{es}\le\phi^{C}_{es}\le L^{1}_{es}\phi^{\max}_{es} \\ a^{C}_{es}\phi^{C(k)}_{es}+b^{C}_{es}T^{C}_{es}+d^{C}_{es}-w^{1}_{es}-w^{2}_{es}, & \phi^{\min}_{es}\le\phi^{C}_{es}\le L^{2}_{es}\phi^{\max}_{es} \end{cases} \\ f^{C(k)}_{es}=(P^{C(k)}_{es}+\phi^{C(k)}_{es})/(q_{\mathrm{gas}}\eta^{C}_{es}) \end{cases} \tag{21}$$

3: ***HSO.*** According to $\phi^{C(k)}_{es}$, solve heating EFC problem (22) and obtain $P^{p(k)}$, $\phi^{C(k)}_{hs}$. Then, pass $P^{p(k)}$ to the ESO.

$$[P^{p(k)},\phi^{C(k)}_{hs}]_h=\arg\{\mathrm{F}_h(\phi^{C(k)}_{es})=0\} \tag{22}$$

4: ***EH at heating slack node.*** Solve Eq. (23) and obtain $f^{C(k)}_{hs}$, $P^{C(k)}_{hs}$. Then, pass $f^{C(k)}_{hs}$ and $P^{C(k)}_{hs}$ to the GSO and ESO.

$$\begin{cases} P^{C(k)}_{hs}=\begin{cases} a^{C}_{hs}\phi^{C(k)}_{hs}+b^{C}_{hs}T^{C}_{hs}+d^{C}_{hs}, & L^{1}_{hs}\phi^{\max}_{hs}\le\phi^{C}_{hs}\le\phi^{\max}_{hs} \\ a^{C}_{hs}\phi^{C(k)}_{hs}+b^{C}_{hs}T^{C}_{hs}+d^{C}_{hs}-w^{1}_{hs}, & L^{2}_{hs}\phi^{\max}_{hs}\le\phi^{C}_{hs}\le L^{1}_{hs}\phi^{\max}_{hs} \\ a^{C}_{hs}\phi^{C(k)}_{hs}+b^{C}_{hs}T^{C}_{hs}+d^{C}_{hs}-w^{1}_{hs}-w^{2}_{hs}, & \phi^{\min}_{hs}\le\phi^{C}_{hs}\le L^{2}_{hs}\phi^{\max}_{hs} \end{cases} \\ f^{C(k)}_{hs}=(P^{C(k)}_{hs}+\phi^{C(k)}_{hs})/(q_{\mathrm{gas}}\eta^{C}_{hs}) \end{cases} \tag{23}$$

5: ***GSO.*** According to $f^{C(k)}_{hs}$ and $f^{C(k)}_{es}$, solve gas EFC problem (24) and obtain $P^{comp(k)}$. Then, pass $P^{comp(k)}$ to the ESO.

$$[P^{comp(k)}]_g=\arg\left\{\mathrm{F}_g\left(f^{C(k)}_{hs},f^{C(k)}_{es}\right)=0\right\} \tag{24}$$

6: ***ESO.*** According to $P^{comp(k)}$, $P^{p(k)}$ and $P^{C(k)}_{hs}$, solve the electrical EFC problem (25) and obtain $P^{C(k+1)}_{es}$.

$$[P^{C(k+1)}_{es}]_e=\arg\{\mathrm{F}_e(P^{comp(k)},P^{p(k)},P^{C(k)}_{hs})=0\} \tag{25}$$

7: If $|P^{C(k+1)}_{es}-P^{C(k)}_{es}|\le\varepsilon$, the iterative algorithm converges; Else, k=k+1, and repeat from step 2.

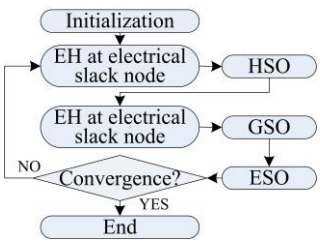

Fig. 4-a. The diagram of the FPDSM.

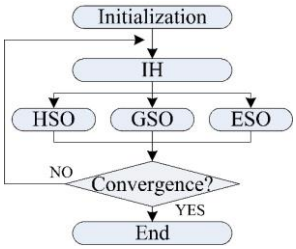

Fig. 4-b. The diagram of the FPDPM

In ***Structure (b)***, the subsystem operators, i.e., the ESO, GSO and HSO, simultaneously exchange information with an IH in a radial structure. Consequently, a novel FPDPM is proposed where the EFC in subsystems can be carried out in parallel based on the information exchange from the IH. The detailed FPDPM and information flow are shown in Algorithm 2 and Fig. 4-b, as shown in radial diagram of Fig. 3-b.

Algorithm 2: The FPDPM based on *Structure (b)*.

1: ***Initialization*.** Define tolerance ε, the indices of iterations k=0; pre-estimate the initial value related to additional known variables, i.e., ($\phi_{hs}^{C(0)}$, $P^{p(0)}$) by the HSO, $P_{es}^{C(0)}$ by the ESO, and $P^{comp(0)}$ by the GSO. Then, pass them to the IH.

2: ***IH*.** By solving Eqns. (21) and (23), translate ($\phi_{hs}^{C(k)}$, $P^{p(k)}$, $P_{es}^{C(k)}$, $P^{comp(k)}$) to ($P^{comp(k)}$, $P^{p(k)}$, $P_{hs}^{C(k)}$) for the ESO, $\phi_{es}^{C(k)}$ for the HSO, ($f_{es}^{C(k)}$, $f_{hs}^{C(k)}$) for the GSO. Then, pass them to the ESO, HSO, and GSO, respectively.

3: ***ESO*, *GSO and HSO*.** Update ($\phi_{hs}^{C(k+1)}$, $P^{p(k+1)}$), ($P_{es}^{C(k+1)}$) and ($P^{comp(k+1)}$) by solving (26), (27) and (28), respectively. Then, pass them to the IH.

$$[P^{p(k+1)},\phi_{hs}^{C(k+1)}]_h=\arg\{\mathrm{F}_h(\phi_{es}^{C(k)})=0\} \quad (26)$$

$$[P_{es}^{C(k+1)}]_e=\arg\{\mathrm{F}_e(P^{comp(k)},P^{p(k)},P_{hs}^{C(k)})=0\} \quad (27)$$

$$[P^{comp(k+1)}]_g=\arg\{\mathrm{F}_g(f_{hs}^{C(k)},f_{es}^{C(k)})=0\} \quad (28)$$

4: If $\max\{|\phi_{hs}^{C(k+1)}-\phi_{hs}^{C(k)}|, |P^{p(k+1)}-P^{p(k)}|, |P_{es}^{C(k+1)}-P_{es}^{C(k)}|, |P^{comp(k+1)}-P^{comp(k)}|\} \le \varepsilon$, the iterative algorithm converges; Else, k=k+1, and repeat from step 2.

In Algorithm 1 and Algorithm 2, linear equations (21) and (23) can be solved directly, and nonlinear equations related to EFC in subsystems (22) and (24)-(28) can be solved with the Newton-Raphson technique [12].

D. Sufficient Conditions for Convergence

1) FPDSM. FPDSM solves the EFC problem in MESs by the fixed-point iterative formulation (29), where x denotes the variable P_{es}^{C} at the fixed-point; and $\Phi(x)$ are energy flow equations in the MES model. According to the fixed-point principle, we propose **Theorem 1** for the convergence of formulation (29). The proof for **Theorem 1** is presented in Appendix A.

$$x^{(k+1)}=\Phi(x^{(k)}) \quad (29)$$

Theorem 1: The iterative formulation (29) can converge to a fixed-point x^* when $\Phi(x)$ satisfies two conditions: 1) the derivative of $\Phi(x)$ with respect to x, i.e., $\Phi'(x)$, is continuous in a neighborhood of x^*, and 2) $|\Phi'(x^*)|\le L<1$. Besides, given the convergence accuracy ε, (29) can converge to the fixed-point x^* within finite iterations of $\log_L(|x^0-x^*|/\varepsilon)$.

Based on **Theorem 1**, the sufficient conditions for convergence of FPDSM are presented. Firstly, a neighborhood of x^* exists where the energy flow direction remains unchanged, thereby ensuring the continuity of $\Phi'(x)$ in this neighborhood to meet condition 1) in **Theorem 1**. Subsequently, the condition 2) in **Theorem 1**, i.e., $|\Phi'(x^*)|<1$, i.e., is derived as follows. First, the active load balance for electricity systems is drawn in (30).

$$P_{es}^{C}=P^{p}(P_{es}^{C})+P^{comp}(P_{es}^{C})+P^{le}+P^{loss}(P_{es}^{C})-P_{hs}^{C}(P_{es}^{C})-P^{ge}=\Phi(P_{es}^{C}) \quad (30)$$

where P^{loss} is the power loss of whole networks; and P^{ge} is the power generated by the units except for those at electrical and heating slack nodes. Then, $\Phi'(P_{es}^{C})$ is derived as shown in (31).

$$\Phi'(P_{es}^{C})=-(P_{hs}^{C})'+(P^{p})'+(P^{comp})'+(P^{loss})' \quad (31)$$

According to Theorem 1, the FPDSM will converge to P_{es}^{C*} if $|\Phi'(P_{es}^{C*})|<1$, which serves as the sufficient condition for the FPDSM convergence. However, deriving the analytic expression of $\Phi'(P_{es}^{C*})$ is a considerable challenge because of the implicit equations in $\Phi(P_{es}^{C})$ and separate management of MESs. In this paper, the value of $\Phi'(P_{es}^{C*})$ is derived by conducting the heating, gas and electrical EFC under different value P_{es}^{C}, thereby generating the sensitivity of (P_{hs}^{C}, P^{p}, P^{comp}, P^{loss}) to P_{es}^{C}. During this process, the value of $[(P_{hs}^{C})']$, $[(P^{p})']$, $[(P^{comp})']$ and $[(P^{loss})']$ can be estimated by HSO, GSO and ESO, respectively.

2) FPDPM. In FPDPM, the iteration formula (32) is derived to calculate the fixed-point $\boldsymbol{x}^*$, where $\boldsymbol{x}=[P_{es}^{C}, \phi_{hs}^{C}, P^{p}, P^{comp}]^{\mathrm{T}}$; $\boldsymbol{\Phi}(\boldsymbol{x})$ is denoted as $[\Psi_1, \Psi_2, \Psi_3, \Psi_4]^{\mathrm{T}}$; and the detailed structure of $\boldsymbol{x}$ and $\boldsymbol{\Phi}(\boldsymbol{x})$ is introduced in Appendix B. **Theorem 2** is obtained based on fixed-point principle for the convergence of the formula (32), and the proof for **Theorem 2** is presented in Appendix C.

$$\boldsymbol{x}^{(k+1)}=\boldsymbol{\Phi}(\boldsymbol{x}^{(k)}) \quad (32)$$

Theorem 2: The iteration formula (32) can converge to a fixed point $\boldsymbol{x}^*$ when $\boldsymbol{\Phi}(\boldsymbol{x})$ satisfies: 1) $\boldsymbol{\Phi}(\boldsymbol{x})$ is differentiable in a neighborhood of $\boldsymbol{x}^*$, and 2) the spectral radius of matrix $\boldsymbol{\Phi}'(\boldsymbol{x}^*)$, denoted as μ, is less than 1. Besides, given the convergence accuracy ε, (32) can converge to the fixed-point $\boldsymbol{x}^*$ within finite iterations of $\log_L(\|\boldsymbol{x}^0-\boldsymbol{x}^*\|_\xi/\varepsilon)$, where $L=\mu+2\xi\le1$, and ξ is a small number.

According to **Theorem 2**, the sufficient conditions for convergence of FPDPM are presented. The differentiability of $\boldsymbol{\Phi}(\boldsymbol{x})$ has been analyzed in Section IV-D-1, which meets condition 1) in **Theorem 2**, and then the spectral radius of $\boldsymbol{\Phi}'(\boldsymbol{x}^*)$ is calculated to meet condition 2) in **Theorem 2**.

Firstly, the elements of $\boldsymbol{\Phi}'(\boldsymbol{x})$ are calculated in (33).

$$\begin{aligned}
&\frac{\partial\Psi_1}{\partial\phi_{hs}^{C}}=\frac{\partial\Psi_e}{\partial\phi_{hs}^{C}}-\frac{\partial P_{hs}^{C}}{\partial\phi_{hs}^{C}}=\omega_1-a_{hs}^{C},\ \frac{\partial\Psi_1}{\partial P^{p}}=\frac{\partial P^{p}}{\partial P^{p}}+\frac{\partial\Psi_e}{\partial P^{p}}=1+\omega_2\\
&\frac{\partial\Psi_1}{\partial P^{comp}}=\frac{\partial P^{comp}}{\partial P^{comp}}+\frac{\partial\Psi_e}{\partial P^{comp}}=1+\omega_3,\ \frac{\partial\Psi_2}{\partial P_{es}^{C}}=\frac{\partial\Psi_h^{C}}{\partial P_{es}^{C}}=\omega_4\\
&\frac{\partial\Psi_3}{\partial P_{es}^{C}}=\frac{\partial\Psi_h^{p}}{\partial P_{es}^{C}}=\omega_5,\ \frac{\partial\Psi_4}{\partial P_{es}^{C}}=\frac{\partial\Psi_g}{\partial P_{es}^{C}}=\omega_6,\ \frac{\partial\Psi_4}{\partial\phi_{hs}^{C}}=\frac{\partial\Psi_g}{\partial\phi_{hs}^{C}}=\omega_7
\end{aligned} \quad (33)$$

Then, the structure of $\boldsymbol{\Phi}'(\boldsymbol{x})$ can be formulated as (34).

$$\boldsymbol{\Phi}'(\boldsymbol{x})=\begin{bmatrix}\frac{\partial\Psi_1}{\partial P_{es}^{C}} & \frac{\partial\Psi_1}{\partial\phi_{hs}^{C}} & \frac{\partial\Psi_1}{\partial P^{p}} & \frac{\partial\Psi_1}{\partial P^{comp}}\\ \frac{\partial\Psi_2}{\partial P_{es}^{C}} & \frac{\partial\Psi_2}{\partial\phi_{hs}^{C}} & \frac{\partial\Psi_2}{\partial P^{p}} & \frac{\partial\Psi_2}{\partial P^{comp}}\\ \frac{\partial\Psi_3}{\partial P_{es}^{C}} & \frac{\partial\Psi_3}{\partial\phi_{hs}^{C}} & \frac{\partial\Psi_3}{\partial P^{p}} & \frac{\partial\Psi_3}{\partial P^{comp}}\\ \frac{\partial\Psi_4}{\partial P_{es}^{C}} & \frac{\partial\Psi_4}{\partial\phi_{hs}^{C}} & \frac{\partial\Psi_4}{\partial P^{p}} & \frac{\partial\Psi_4}{\partial P^{comp}}\end{bmatrix}=\begin{bmatrix}0 & \omega_1-a_{hs}^{C} & \omega_2+1 & \omega_3+1\\ \omega_4 & 0 & 0 & 0\\ \omega_5 & 0 & 0 & 0\\ \omega_6 & \omega_7 & 0 & 0\end{bmatrix} \quad (34)$$

Lastly, the eigenvalue of matrix $\boldsymbol{\Phi}'(\boldsymbol{x})$, i.e., λ_1, λ_2, λ_3 and λ_4, can be obtained by solving (35) using the Cardans formula. Hence, the spectral radius of $\boldsymbol{\Phi}'(\boldsymbol{x}^*)$ is the value of $\max\{|\lambda_1|, |\lambda_2|, |\lambda_3|, |\lambda_4|\}$, and the sufficient condition for FPDPM is to meet $\max\{|\lambda_1|, |\lambda_2|, |\lambda_3|, |\lambda_4|\}<1$.

$$\lambda\cdot[\lambda^3-(\omega_3\omega_6+\omega_6+\omega_2\omega_5+\omega_5+\omega_1-a_{hs}^{c})\cdot\lambda-\omega_4\omega_7(\omega_3+1)]=0 \quad (35)$$

This article has been accepted for publication in a future issue of this journal, but has not been fully edited. Content may change prior to final publication. Citation information: DOI 10.1109/TSTE.2020.2966737, IEEE Transactions on Sustainable Energy

E. Value Estimation for Unknown Variables

In Algorithm 1 and 2, additional unknown variables need to be estimated for the initialization of FPDSM and FPDPM. In addition, the estimation of general unknown variables is also required in Newton-Raphson technique for the EFC in sub-systems. The variables to be estimated with corresponding algorithm are summarized in Table II. The procedure used to estimate these variables is introduced in Fig. 5.

TABLE II VARIABLES TO BE ESTIMATED FOR ALGORITHM INITIALIZATION

	Additional unknown variables		General unknown variables		
Variables	P_{es}^{C}	ϕ_{hs}^{C}, P^{p}, P_{es}^{C}, P^{comp}	$\lvert V\rvert$, θ	T^{s}, T^{r}, m	ρ
Algorithm	FPDSM	FPDPM	Electrical EFC	Heating EFC	Gas EFC

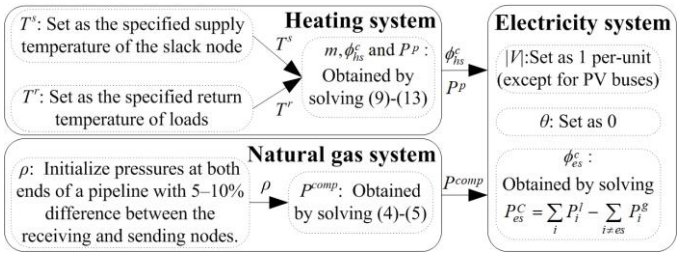

Fig. 5. Initial value estimation for unknown variables

F. Superiority of the Proposed Method

In this section, the proposed method is compared with the independent EFC and UNM methods in terms of computation time, information exchange and solution accuracy. Moreover, the numerical tests will be conducted in Section V-C to verify the conclusions in this section.

1) Superiority over UNM in computational efficiency. It is noted that the computation time for performing EFC in the electricity system with N_e^{total} equations, the gas system with N_g^{total} equations and the heating system with N_h^{total} equations are T_e, T_g and T_h, respectively. In addition, the iteration number of the FPDSM and FPDPM is K_{DSM} and K_{DPM}, respectively. Therefore, the total computation time of the FPDSM and FPDPM is $K_{DSM}\times(T_e+T_g+T_h)$ and $K_{DPM}\times max\{T_e, T_g, T_h\}$, respectively. In comparison, the number of equations in UNM method is $N^{total}=N_e^{total}+N_g^{total}+N_h^{total}+N_{coup}$, where N_{coup} is the number of coupling equations. Based on the proposed distributed framework, the EFC in an MES with N^{total} equations is decomposed into three EFCs with N_e^{total}, N_g^{total} and N_h^{total} equations, respectively. Consequently, the computational efficiency can be improved, with further numerical tests in Section V-C.

2) Superiority over UNM in information exchange. In the UNM, intensively sharing large amounts of information from various sub-systems is a considerable challenge. In contrast, in the FPDSM, the variables to be exchanged among the ESO, GSO and HSO in the k^{th} iteration are $\phi_{es}^{C(k)}$, $f_{es}^{C(k)}$, $P^{p(k)}$, $f_{hs}^{C(k)}$, $P_{hs}^{C(k)}$ and $P^{comp(k)}$, and the numbers of these variables are 1, 1, N_h^p,1,1 and N_g^c, respectively. Hence, the total number of exchanged variables in the FPDSM is $K_{DSM}\times(4+N_h^p+N_g^c)$, while the total number of variables to be exchanged in the FPDPM is $K_{DPM}\times(6+2\cdot N_h^p+2\cdot N_g^c)$. It can be seen that the communication burden of the propsed method can be significantly reduced. Moreover, less information exchange will bring more reliability under the situation of the possible data loss. This conclusion will be validated in Section V-C.

3) Superiority over the independent EFC method in accuracy. In the independent EFC method, there is no coordination between subsystem operators. In this case, additional unknown variables are first estimated by corresponding subsystem operators, and then the energy flow distribution can be calculated by subsystem operators. Therefore, the solution obtained from the independent EFC method is solely dependent on the value of pre-estimated additional unknown variables. In comparison, the proposed method can keep refining the value of additional unknown variables in the iterative solution process, thereby generating more accurate energy flow distribution. Such conclusion will be numerically validated in Section V-C.

G. Discussion

1) Adaptable to other coupling relationships. A comprehensive coupling relationship has been taken as an example to introduce the distributed framework, in which the electrical and heating systems are coupled by the CHP at most of nodes. It should be pointed out that the PPDSM and FPDPM are also suitable for other coupling relationships. For instance, considering a scenario that electrical and heating slack nodes are powered by a GT and a CHP, respectively. In this case, there is no additional variables in the heating system, which means the heating EFC can be conducted independently. By firstly giving the heating power distribution, the EFCs in electrical and gas subsystems can be conducted sequentially or in parallel based on the FPDSM or FPDPM, respectively. Other coupling scenarios can also be studied in a similar approach.

2) Application scope. According to the Theorem 1 and Theorem 2 in Section IV-D, the proposed method can converge to the fixed point under sufficient conditions. In theory, these sufficient conditions can be met for other practical MESs by properly designing the consumption coefficients of CHPs. Taking sufficient conditon (31) as an example, the value of P^{loss}, P^p and P^{comp} is determined by the energy flow distribution in electrical, heating and gas systems, respectively. However, a single CHP at the electrical slack node has little effect on the energy flow distribution in these energy subsystems [17], hence, the value of $(P^{loss})'$, $(P^p)'$ and $(P^{comp})'$ is expected to be small. Then, if either electrical or heating slack node is not powered by CHPs, the value of $(P_{hs}^C)'$ is 0. In these cases, $|\Phi'(P_{es}^{C*})|\approx 0<1$, which guarantees the convergence of the proposed method. If both electrical and heating slack nodes are powered by CHPs, the value of $(P_{hs}^C)'$ can be calculated by (36). It can be seen that when the heating loss is ignored, $\partial\phi_{hs}^C/\partial\phi_{es}^C\approx 0$, and $(P_{hs}^C)'$ is determined by a_{hs}^C/a_{es}^C. In this case, when $a_{hs}^C<a_{es}^C$, i.e., $|\Phi'(P_{es}^{C*})|<1$, the proposed method can converge to the fixed point. Consequently, the convergence of the proposed method can be guaranteed by properly designing parameters of CHPs.

$$\frac{\partial P_{hs}^C}{\partial P_{es}^C}=\frac{\partial P_{hs}^C}{\partial \phi_{hs}^C}\cdot\frac{\partial \phi_{hs}^C}{\partial \phi_{es}^C}\cdot\frac{\partial \phi_{es}^C}{\partial P_{hs}^C}=a_{hs}^C\cdot\frac{\partial \phi_{hs}^C}{\partial \phi_{es}^C}\cdot\frac{1}{a_{es}^C} \tag{36}$$

This article has been accepted for publication in a future issue of this journal, but has not been fully edited. Content may change prior to final publication. Citation information: DOI 10.1109/TSTE.2020.2966737, IEEE Transactions on Sustainable Energy

V. Case Studies and Simulations

To demonstrate the effectiveness of the proposed distributed method, several case studies are implemented in a test MES [20]. All simulations are performed using MATLAB on a computer with a core i5, 3.2 GHz processor and 4 GB RAM.

A. Simulation Parameters

The test MES is shown in Fig. 6, which contains a) the 14-bus electricity system, b) the 14-bus heating system, c) the 20-bus natural gas system and d) 5 coupling EHs. The rated power of the CHP in heating and electricity subsystems are 28.4 MW and 11.2562 MW, respectively [27]. In the electrical network [29], E1 represents the slack node, which is powered by a CHP and a GT via EH-2. In the gas network [30], the gas compressor at node G9 runs with a given compression ratio of 1.05, and the electrical compressor at node G18 runs with a given output pressure of 63 bar, which are powered by the bus E14. In the heating network, H1 represents the slack node, which is powered by a CHP and a GB via EH-1. In addition, each heating source is equipped with a pump powered by the connected electrical nodes.

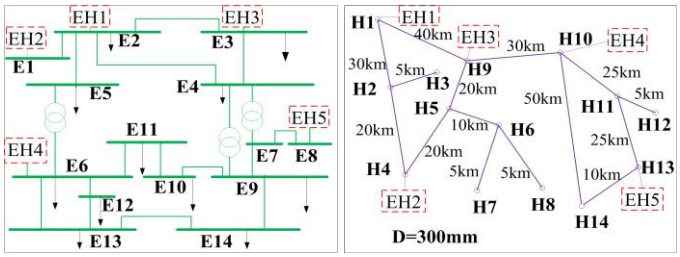

a) The IEEE 14-bus electricity system b) The 14-bus heating system

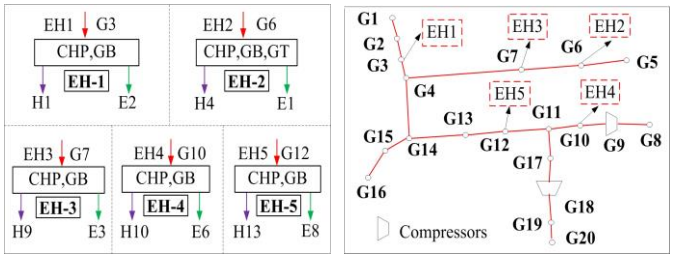

c) The 20-bus natural gas system d) The EHs

Fig. 6. An integrated electricity-gas-heat system

B. Effectiveness of the Distributed Method

It is assumed that the CHP at the slack nodes has priority to be applied due to its high efficiency. If the capacity of the CHP is insufficient to fill energy gaps, the GT at E1 and the GB at H1 are put into operation to generate the remaining power.

To demonstrate the effectiveness of the proposed methods, the most complicated scenario are first studied, i.e., the CHPs in EH1 and EH2 are presumed to be in operation, denoted as ***case 1***. In ***case 1***, the electrical EFC comprises 22 unknown variables and 22 equations, i.e., Eqs. (1)-(2) with the number of 13 and 9, respectively. Similarly, the gas EFC model includes 18 unknown pressure variables and 18 Eqs. (3). The heating EFC model contains 62 unknown variables and 62 equations, i.e., Eqs. (7)-(12) with the number of 14, 14, 9, 9, 14 and 2, respectively. The additional unknown variables are (P^{comp}, P^{p}, P^{C}_{hs}) for the ESO, (ϕ^{C}_{es}) for the HSO and (f^{C}_{es}, f^{C}_{hs})for the GSO, with the number of (1,5,1), (1) and (1,1), respectively. Then, the FPDSM, FPDPM and UNM are implemented respectively to carry out the EFCs. The FPDSM and FPDPM can converge after 6 and 9 iterations, respectively. Specifically, in this case, the electrical power generated by the CHP at E1 is P^{C}_{es}=10.2722 MW, which is within the rated electrical power of the CHP, i.e., 11.2562 MW. However, the heating power drawn from the CHP at H1 is ϕ^{C}_{hs} =37.8926 MW, which exceeds the rated heating power of the CHP, i.e., 28.4 MW. Hence, the heating demand and losses cannot be met only by a CHP at the heating slack node H1. Consequently, the GB at H1 is put in operation while the CHP at H1 is running at the rated power. Therefore, a new scenario is developed, denoted as ***case 2***. Similarly, the FPDSM, FPDPM and UNM are implemented to carry out the EFC, and the simulation results are shown in Tables III-VI.

TABLE III Power Flow Distribution in the Electricity System

Node	Active power Load-1/CHP (MW)	Active power Load-2 (MW)	Reactive power Load (MVar)	Voltage magnitude (p.u.) / angle (°)
E1	2.5000/10.3156	0.5494	0	1.0600/ 0
E2	3.4720/11.2562	0.8842	2.0320	1.0450/0.1121
E3	15.0720/7.1670	0.4269	3.0400	1.0100/0.0380
E4	7.6480	0	-0.6240	1.0391/-0.1958
E5	1.2160	0	0.2560	1.0386/-0.0370
E6	1.9720/9.6820	0.4429	1.2000	1.0700/0.2253
E7	0	0	0	1.0833/0.0134
E8	0/9.6820	0.4466	0	1.0900/0.8028
E9	4.7200	0	2.6560	1.0902/-0.3723
E10	1.4400	0	0.9280	1.0855/-0.3242
E11	0.5600	0	0.2880	1.0773/-0.0882
E12	0.9760	0	0.2560	1.0694/0.0622
E13	2.1600	0	0.9280	1.0700/-0.0132
E14	2.3840	0.6496	0.8000	1.0782/-0.4204

Specifically, the power flow in the electricity system is shown in Table III, where load-1 represents the general electric load, and load-2 denotes pumps and electric compressors. It can be seen that the active power supplied by the CHP at the electric slack node E1 is 10.3156 MW, which is within the rated power of the CHP, i.e., 11.2562 MW. Then, the gas flow distribution in the gas system is shown in Table IV, where the total general gas load of 46.2980×10^{6} m^3/day and the multi-energy load of 0.5328×10^{6} m^3/day are met. Furthermore, to pressurize the gas flow, the gas-consuming compressor at G9 should consume a gas flow of 3.8509×10^{3} m^3/day, while the electricity consuming compressor at G18 should be powered by E14 with 0.6496 MW. In addition, the heating flow distribution is shown in Table V. It can be seen that the CHP and GB at the heating slack node H1 generate heating power of 28.4 MW and 9.3302 MW, respectively. Consequently, the heating power losses incurred in the water supply and return process can be compensated, i.e., ϕ^{s}_{loss} =6.7963 MW and ϕ^{r}_{loss}=2.3025 MW, and the detailed heat losses , the water mass m_{ij} and pressure losses Δp_{ab} are shown in Table VI. The pressure losses are compensated by the pumps powered by the electricity system.

TABLE IV Gas Flow Distribution in the Gas System

Node	f^{s}_{n}/ f^{l}_{n} ($\times10^{6}$ m^3/day)	f^{C} ($\times10^{3}$ m^3/day)	f^{B} ($\times10^{3}$ m^3/day)	f^{comp} ($\times10^{3}$ m^3/day)	ρ (bar)
G1	8.9571/0	0	0	0	55.8229
G2	8.4000/0	0	0	0	55.8031
G3	0/3.9180	99.8376	25.8384	0	55.6914
G4	0/0	0	0	0	54.5391
G5	2.8147/0	0	0	0	53.3419

This article has been accepted for publication in a future issue of this journal, but has not been fully edited. Content may change prior to final publication. Citation information: DOI 10.1109/TSTE.2020.2966737, IEEE Transactions on Sustainable Energy

G6	0/4.0340	95.7072	13.8466	0	52.5960
G7	0/5.2560	80.5672	8.3079	0	52.7088
G8	24.4990/0	0	0	0	59.8520
G9	0/0	0	0	3.8509	62.2656
G10	0/6.3650	92.7504	5.5386	0	60.1188
G11	0/0	0	0	0	58.6200
G12	0/2.1200	92.7504	13.8466	0	56.0712
G13	1.2000/0	0	0	0	54.2045
G14	0.9600/0	0	0	0	53.9229
G15	0/6.8480	0	0	0	52.6174
G16	0/15.6160	0	0	0	50.9956
G17	0/0	0	0	0	57.8550
G18	0/0	0	0	0	63.0000
G19	0/0.2220	0	0	0	35.7444
G20	0/1.9190	0	0	0	33.8420

TABLE V HEATING FLOW DISTRIBUTION IN THE HEATING SYSTEM

Node	T^s (°C)	T^r(°C)	ϕ^C (MW)	ϕ^B (MW)	ϕ^I (MW)
H1	127.2780	47.7527	28.4000	9.3302	0
H2	124.6687	49.1615	0	0	0
H3	124.1036	50.0000	0	0	15.0000
H4	126.7665	49.5267	26.3685	5.0000	25.0000
H5	123.7269	49.5392	0	0	0
H6	123.0726	49.7690	0	0	0
H7	122.5272	50.0000	0	0	15.0000
H8	122.2582	50.0000	0	0	10.0000
H9	126.1518	48.5177	20.0000	3.0000	10.0000
H10	126.8109	48.3592	25.0000	2.0000	15.0000
H11	123.3854	48.6364	0	0	0
H12	122.5656	50.0000	0	0	10.0000
H13	126.5282	49.8086	25.0000	5.0000	25.0000
H14	1203481	50.0000	0	0	15.0000

Then, the value of $\Phi'(x)$ for FPDSM in ***case 2*** is calculated to verify the effectiveness of sufficient conditions. In this case, $(P_{hs}^C)'=0$, and the sensitivity of (P^p, P^{comp}, P^{loss}) to P_{es}^C is presented in Fig. 7. It can be obtained from Fig.7 that $\partial P^P/\partial P_{es}^C \approx -0.046298$, $\partial P^{comp}/\partial P_{es}^C \approx 2\times10^{-5}$, $\partial P^{loss}/\partial P_{es}^C \approx 9.4\times10^{-5}$. Then, $|\Phi'(P_{es}^C)| = |-\partial P_{hs}^C/\partial P_{es}^C + \partial P^P/\partial P_{es}^C + \partial P^{comp}/\partial P_{es}^C + \partial P^{loss}/\partial P_{es}^C| \approx |0-0.046298+2\times10^{-5}+9.4\times10^{-5}| \approx 0.046$, i.e., $|\Phi'(x)| \approx 0.046<1$. Similarly, the eigenvalue of matrix $\boldsymbol{\Phi}'(\boldsymbol{x})$ in FPDPM is 0.2145, which is also less than 1 in this MES. Consequently, the convergence of FPDSM and FPDPM can be guaranteed.

TABLE VI WATER MASS, HEAT LOSSES AND PRESSURE LOSSES

Line *a-b*	m_{ij}(kg/s)	ϕ_{loss}^i (MW)	ϕ_{loss}^i (MW)	Δp_{ab} (bar)
1-2	63.7645	0.6958	0.2323	12.1917
2-3	48.4025	0.1144	0.0399	1.1714
2-4	15.3620	0.4447	0.1533	0.4720
4-5	32.8066	0.4603	0.1559	2.1525
5-6	82.5469	0.2268	0.0793	6.8140
6-7	49.4546	0.1128	0.0399	1.2229
6-8	33.0923	0.1127	0.0399	0.5476
5-9	49.7403	0.4602	0.1566	4.9482
1-9	49.6842	0.9204	0.3023	9.8741
9-10	37.2714	0.6837	0.2258	4.1675
10-11	40.1691	0.5754	0.1903	4.0339
11-12	32.9523	0.1130	0.0399	0.5429
11-13	7.2167	0.5225	0.1834	0.1302
13-14	20.6819	0.2304	0.0791	0.4277
10-14	30.3046	1.1232	0.3846	4.5918

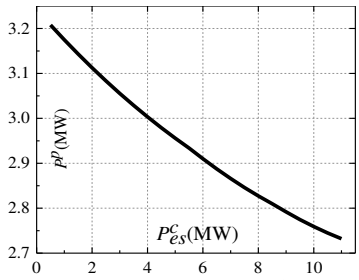

Fig.7a The sensitivity of P^p to P_{es}^C

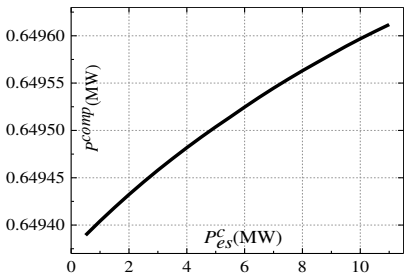

Fig.7b The sensitivity of P^{comp} to P_{es}^C

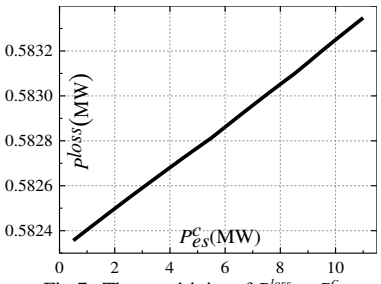

Fig.7c The sensitivity of P^{loss} to P_{es}^C

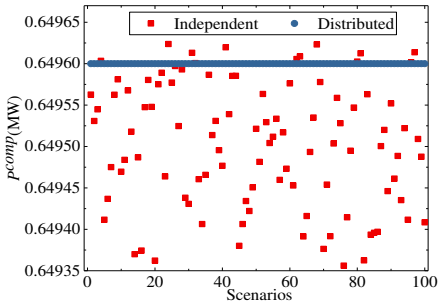

Fig.8a The value of P^{comp} in 100 scenarios.

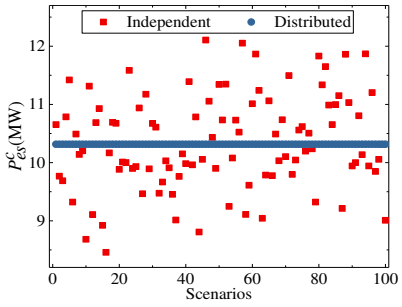

Fig.8b The value of P_{es}^C in 100 scenarios.

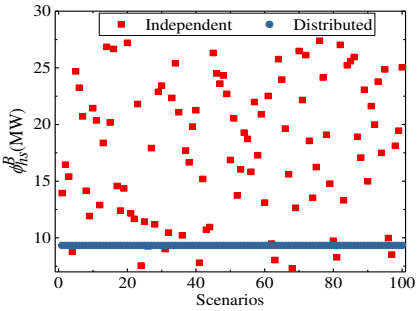

Fig.8c The value of ϕ_{hs}^B in 100 scenarios.

C. Superiority of the Proposed Method in Case Studies

In this section, by performing numerical tests in the MES, the superiority of the distributed method over independent EFC method and UNM method is demonstrated in terms of accuracy, computational efficiency and robustness.

1) Superiority over independent EFC method

100 scenarios are generated with random initial value of additional unknown variables, these numerical tests are performed in ***Case 2*** with the proposed distributed method and the independent methods. Specifically, the pre-estimated power of the CHP varies from 0 to the rated value, and the forecasted errors of other pre-estimated variables range from -100% to +100%. 100 sets of initial values are selected randomly, and based on these simulation conditions, the value of P^{comp}, P_{es}^C and ϕ_{hs}^B in 100 scenarios are shown in Fig. 8.

It can be seen that the proposed distributed method can consistently converge to the accurate solution regardless of randomness in initial values. In comparison, the solution from the independent method is inaccurate with the maximum error of 2.5×10^{-4} MW for P^{comp}, 1.8MW for P_{es}^C and 18.2 MW for ϕ_{hs}^B,

This article has been accepted for publication in a future issue of this journal, but has not been fully edited. Content may change prior to final publication. Citation information: DOI 10.1109/TSTE.2020.2966737, IEEE Transactions on Sustainable Energy

respectively. This is because the proposed method can adaptively refine the value of variables in iteration process, and thus arrive at more accurate energy flow distribution. However, in the independent method, there is no coordination among subsystem operators. Hence, the solution is fully dependent on the pre-estimated values of each system operators.

2) Superiority over UNM in Computational Efficiency

In this section, the superiority of the distributed method over UNM in computational efficiency is quantified. Firstly, four cases are used to represent different coupling relationships in MESs. Specifically, in addition to ***case 1*** and ***case 2***, two more cases which are ***case 3*** (a GT and a CHP at E1, a CHP at H1) and ***case 4*** (a GT and a CHP at E1, a GB and a CHP at H1) are designed. Then, with random initial values, average computation times of FPDSM, FPDPM and UNM methods in 100 scenarios are shown in Fig. 9.

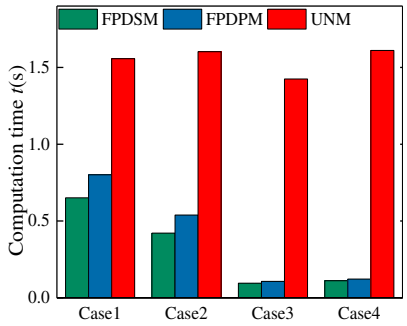

Fig.9 Average computation time of the FPDSM, FPDPM and UNM

As shown in Fig. 9, the computation time of the FPDSM and FPDPM shows considerable advantages over those of the UNM. Specifically, the minimum time of 0.7s can be saved by employing the proposed method. This is because the large-scale EFC problem in an MES is decomposed into three small-scale EFCs in subsystems by the proposed method, and this decomposition efficiently reduces the computaional burden. In addition, the variation in the computation time versus different coupling relationships is further discussed. Specifically, in the UNM, all equations are solved simultaneously, so the coupling relationships have little impact on the computation time. However, in FPDSM and FPDPM, different sequences of EFC in subsystems are applied under various coupling relationships and further lead to variation in computational efficiency.

3) Superiority over UNM in Solution Accuracy

The convergence accuracy is analyzed in this section for FPDSM, FPDPM and UNM methods. As shown in Fig. 10, when the convergence accuracy ε decreases from 10^{-3} to 10^{-8}, the average computation time of the UNM increases by the minimum time of 0.776 s in the four cases, while the average computation times of the FPDSM and FPDPM increase by the maximum time of 0.359 s. It is noted that both UNM and the proposed method can improve the solution accuracy by prolong the computation time. However, the proposed method shows considerable advantages over the UNM in computation time, as demonstrated in Section V-C-2. Consequently, the proposed method needs less computation time to improve its accuracy, and with the same computation time, the convergence accuracy of FPDSM and FPDPM is much higher than that of UNM.

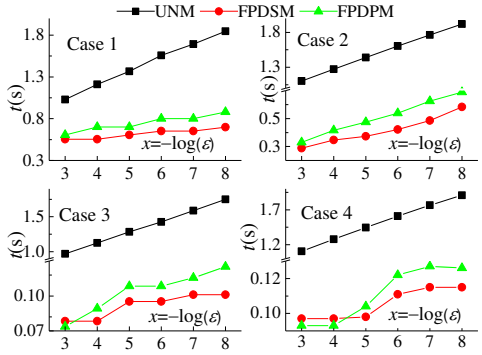

Fig.10 The relationships between computation time and accuracy

4) Superiority over UNM in Robustness

In the UNM, any data loss will lead to EFC non-convergence due to the requirement of whole information sharing. Therefore, assessment of the robustness against data loss in the distributed methods is required. Simulations are performed in 100 scenarios with $\varepsilon=10^{-4}$. The average numbers of iterations for convergence in the FPDSM and FPDPM methods are shown in Table VII, where PRO denotes the probability of the data loss occurrence in each information exchange. It can be seen that FPDSM and FPDPM can always converge to the optimal point after finite iterations but at the expense of larger numbers of iterations with the increasing PRO. It can be seen that the proposed method can withstand data loss in the solution process since once data loss occurs, the data in the last iteration can be utilized until the data transmission is precisely completed. In this case, the computation time is prolonged. Consequently, the robustness against data loss can be efficiently improved by employing the proposed method.

TABLE VII THE ITERATION OF FPDSM AND FPDPM UNDER DIFFERENT PRO

Cases	Methods	PRO									
		0	0.1	0.2	0.3	0.4	0.5	0.6	0.7	0.8	0.9
Case1	FPDSM	3.94	4.08	4.52	4.78	4.94	5.48	6.78	7.78	9.48	15.92
	FPDPM	6.85	6.98	7.17	7.41	7.73	8.12	8.97	10.27	12.54	18.17
Case2	FPDSM	4.57	4.79	5.00	5.50	5.91	6.40	7.19	8.46	11.47	14.84
	FPDPM	7.40	7.52	7.53	8.14	8.19	8.80	9.87	10.57	12.70	19.45
Case3	FPDSM	2.00	2.05	2.27	2.52	2.88	3.29	3.99	4.51	6.12	12.94
	FPDPM	2.73	2.86	3.04	3.28	3.45	4.02	4.68	6.05	8.31	12.39
Case4	FPDSM	2.00	2.11	2.25	2.31	2.77	3.5	3.91	4.66	7.07	10.80
	FPDPM	2.00	2.07	2.28	2.41	2.99	3.32	3.87	4.55	6.43	11.29

VI. CONCLUSION

A novel fixed-point based distributed method for the EFC in MESs is proposed in this paper. The proposed method can adapt to different structures of information exchange among electrical, natural gas and heating subsystems. Moreover, the information privacy of subsystems can be preserved by sharing limited information in the solution process. Based on the fixed point principle, the convergence of the proposed distributed method can be guaranteed, and sufficient conditions for the convergence are presented. Compared with existing EFC methods, the analytical and numerical results demonstrate that the proposed method can converge to an accurate solution with less computation time and more robustness against unknown energy variables and data loss between subsystems. In authors' future work, steady state analysis of MESs will be conducted based on the proposed EFC method.

This article has been accepted for publication in a future issue of this journal, but has not been fully edited. Content may change prior to final publication. Citation information: DOI 10.1109/TSTE.2020.2966737, IEEE Transactions on Sustainable Energy

APPENDIX

A. Proof of Theorem 1

First, under the condition 1) and 2) in Theorem 1, there exists the neighborhood of x^*, denoted as $U(x^*,\delta)$, such that $|\Phi'(x)|\le L<1$, and for all $x \in U(x^*,\delta)$:

$$\left|\Phi(x)-x^*\right|=\left|\Phi(x)-\Phi(x^*)\right|=\left|\Phi'(\varepsilon)\right|\cdot\left|x-x^*\right|\le L\cdot\left|x-x^*\right|<\left|x-x^*\right|<\delta \quad \text{(A1)}$$

Equation (A1) indicate that $\Phi(x)\in U(x^*,\delta)$. Then, for all $x^{(k+1)}=\Phi(x^{(k)})\in U(x^*,\delta)$:

$$\begin{aligned}\left|x^{(k+1)}-x^*\right|&=\left|\Phi(x^{(k)})-\Phi(x^*)\right|=\left|\Phi'(\varepsilon)\right|\cdot\left|x^{(k)}-x^*\right|\\&\le L\cdot\left|x^{(k)}-x^*\right|\le L^2\cdot\left|x^{(k-1)}-x^*\right|\le\bullet\bullet\bullet\le L^{k+1}\cdot\left|x^0-x^*\right|\end{aligned} \quad \text{(A2)}$$

According to (A2), $\lim_{k\to\infty}\left|x^{(k+1)}-x^*\right|\le\lim_{k\to\infty}L^{k+1}\cdot\left|x^0-x^*\right|=0$ is gained, i.e., $\lim_{k\to\infty}x^{(k+1)}=x^*$. That is, sequence $\{x^{(k)}\}$ will converge to the fixed point x^*. Besides, according to (A2), when $L^{k+1}\cdot|x^0-x^*|\le\varepsilon$ is satisfied, i.e., $k+1\le\log_L(|x^0-x^*|/\varepsilon)$, the convergence criterion $|x^{(k+1)}-x^*|\le\varepsilon$ is met. Hence, (29) can converge to the fixed-point x^* after finite iterations of $\log_L(|x^0-x^*|/\varepsilon)$.

B. Structure of (32)

First, the active load balance for electricity systems can be formulated as:

$$P_{es}^{C}=P^{p}+P^{comp}+P^{le}+P^{loss}-P_{hs}^{C}-P^{ge} \quad \text{(A3)}$$

In electricity systems, with the given (ϕ_{hs}^{C}, P^p, P^{comp}), the value of P^{loss} can be obtained by solving electrical models (1)-(2) and (14), and this relationship can be formulated by:

$$P^{loss}=\Psi_e(\phi_{hs}^{C},P^{p},P^{comp}) \quad \text{(A4)}$$

Then, the P^{loss} in the equation (A3) can be replaced by the equation (A4). Therefore, the equation (A3) can be rewritten as:

$$P_{es}^{C}=P^{p}+P^{comp}+P^{le}+\Psi_e(\phi_{hs}^{C},P^{p},P^{comp})-P_{hs}^{C}(\phi_{hs}^{C})-P^{ge}=\Psi_1 \quad \text{(A5)}$$

In the heating system, with the given P_{es}^{C}, the value of ϕ_{hs}^{C} and P^p can be obtained by solving heating models (7)-(13), and these relationships can be formulated as equations (A6) and (A7), respectively.

$$\phi_{hs}^{C}=\Psi_h^{C}(P_{es}^{C})=\Psi_2 \quad \text{(A6)}$$

$$P^{p}=\Psi_h^{p}(P_{es}^{C})=\Psi_3 \quad \text{(A7)}$$

In the natural gas system, with the given (P_{es}^{C}, ϕ_{hs}^{C}), the value of P^{comp} can be obtained by solving gas models (3)-(6) and (14), and this relationship can be formulated as equations (A8).

$$P^{comp}=\Psi_g(P_{es}^{C},\phi_{hs}^{C})=\Psi_4 \quad \text{(A8)}$$

Hence, equation (32) is comprised of (A5)-(A8). Specifically, $\boldsymbol{x}=[P_{es}^{C},\ \phi_{hs}^{C},\ P^{p},\ P^{comp}]^{\mathrm{T}}$, and $\boldsymbol{\Phi}(\boldsymbol{x})=[\Psi_1,\ \Psi_2,\ \Psi_3,\ \Psi_4]^{\mathrm{T}}$.

C. Proof of Theorem 2

Due to $\mu<1$, there exists a small number $\xi>0$ such that $\mu+2\xi=L<1$, and a norm $\|\cdot\|_\xi$ such that $\|\boldsymbol{\Phi}'(\boldsymbol{x}^*)\|_\xi\le\mu+\xi$.

Then, according to the definition of derivative, there exists a neighborhood of $\boldsymbol{x}^*$, denoted as $U(\boldsymbol{x}^*,\delta)$, such that $\forall\ \boldsymbol{x}\in U(\boldsymbol{x}^*,\delta)$, we can obtain:

$$\left\|\boldsymbol{\Phi}(\boldsymbol{x})-\boldsymbol{\Phi}(\boldsymbol{x}^*)-\boldsymbol{\Phi}'(\boldsymbol{x}^*)(\boldsymbol{x}-\boldsymbol{x}^*)\right\|_\xi\le\xi\cdot\left\|\boldsymbol{x}-\boldsymbol{x}^*\right\|_\xi \quad \text{(A9)}$$

Hence, we can obtain:

$$\begin{aligned}\left\|\boldsymbol{\Phi}(\boldsymbol{x})-\boldsymbol{x}^*\right\|_\xi&=\left\|\boldsymbol{\Phi}(\boldsymbol{x})-\boldsymbol{\Phi}(\boldsymbol{x}^*)-\boldsymbol{\Phi}'(\boldsymbol{x}^*)(\boldsymbol{x}-\boldsymbol{x}^*)+\boldsymbol{\Phi}'(\boldsymbol{x}^*)(\boldsymbol{x}-\boldsymbol{x}^*)\right\|_\xi\\&\le\left\|\boldsymbol{\Phi}(\boldsymbol{x})-\boldsymbol{\Phi}(\boldsymbol{x}^*)-\boldsymbol{\Phi}'(\boldsymbol{x}^*)(\boldsymbol{x}-\boldsymbol{x}^*)\right\|_\xi+\left\|\boldsymbol{\Phi}'(\boldsymbol{x}^*)(\boldsymbol{x}-\boldsymbol{x}^*)\right\|_\xi\\&\le(\mu+2\xi)\cdot\left\|\boldsymbol{x}-\boldsymbol{x}^*\right\|_\xi=L\cdot\left\|\boldsymbol{x}-\boldsymbol{x}^*\right\|_\xi\end{aligned} \quad \text{(A10)}$$

Then, for all $\boldsymbol{x}^{(k+1)}=\boldsymbol{\Phi}(\boldsymbol{x}^{(k)})\in U(\boldsymbol{x}^*,\delta)$:

$$\begin{aligned}\left\|\boldsymbol{x}^{(k+1)}-\boldsymbol{x}^*\right\|_\xi&=\left\|\boldsymbol{\Phi}(\boldsymbol{x}^{(k)})-\boldsymbol{\Phi}(\boldsymbol{x}^*)\right\|_\xi\le L\cdot\left\|\boldsymbol{x}^{(k)}-\boldsymbol{x}^*\right\|_\xi\\&\le L^2\cdot\left\|\boldsymbol{x}^{(k-1)}-\boldsymbol{x}^*\right\|_\xi\le\bullet\bullet\bullet\le L^{k+1}\cdot\left\|\boldsymbol{x}^0-\boldsymbol{x}^*\right\|_\xi\end{aligned} \quad \text{(A11)}$$

Hence, we can obtain:

$$\begin{aligned}\left\|\boldsymbol{x}^{(k+p)}-\boldsymbol{x}^{(k)}\right\|_\xi&=\left\|\boldsymbol{x}^{(k+p)}-\boldsymbol{x}^*+\boldsymbol{x}^*-\boldsymbol{x}^{(k)}\right\|_\xi\\&\le\left\|\boldsymbol{x}^{(k+p)}-\boldsymbol{x}^*\right\|_\xi+\left\|\boldsymbol{x}^{(k)}-\boldsymbol{x}^*\right\|_\xi\\&\le L^{k+p}\cdot\left\|\boldsymbol{x}^0-\boldsymbol{x}^*\right\|_\xi+L^k\cdot\left\|\boldsymbol{x}^0-\boldsymbol{x}^*\right\|_\xi\\&=2L^k\cdot\left\|\boldsymbol{x}^0-\boldsymbol{x}^*\right\|_\xi\end{aligned} \quad \text{(A12)}$$

Consequently, $\{\boldsymbol{x}^{(k)}\}$ is a convergent Cauchy sequence, and $\lim_{k\to\infty}\left\|\boldsymbol{x}^{(k+1)}-\boldsymbol{x}^*\right\|_\xi\le\lim_{k\to\infty}L^{k+1}\cdot\left\|\boldsymbol{x}^0-\boldsymbol{x}^*\right\|_\xi=0$, i.e., $\lim_{k\to\infty}\boldsymbol{x}^{(k+1)}=\boldsymbol{x}^*$. That is, the sequence $\{\boldsymbol{x}^{(k)}\}$ will converge to the fixed point $\boldsymbol{x}^*$. Besides, according to (A11), when $L^{k+1}\cdot\|\boldsymbol{x}^0-\boldsymbol{x}^*\|_\xi\le\varepsilon$ is satisfied, i.e., $k+1\le\log_L(\|\boldsymbol{x}^0-\boldsymbol{x}^*\|_\xi/\varepsilon)$, the convergence criterion $\|\boldsymbol{x}^{(k+1)}-\boldsymbol{x}^*\|_\xi\le\varepsilon$ is met. Hence, (32) can converge to the fixed-point $\boldsymbol{x}^*$ after finite iterations of $\log_L(\|\boldsymbol{x}^0-\boldsymbol{x}^*\|_\xi/\varepsilon)$.

REFERENCES

[1] A. Quelhas and J.D. Mccalley, "A Multiperiod Generalized Network Flow Model of the U.S. Integrated Energy System: Part I—Model Description," *IEEE Trans. Power Syst*., vol. 22, no. 2, pp. 829-836, May 2007.

[2] A. Huang, *et al*., "The Future Renewable Electric Energy Delivery and Management (FREEDM) System: The Energy Internet," *Proceedings of the IEEE*, vol. 99, no. 1, pp. 133-148, Jan. 2011.

[3] J. Rifkin, The Third Industrial Revolution: How Lateral Power Is Transforming Energy the Economy and the World St. Martin's Press, pp. 1-30, 2011.

[4] R. Lund and B.V. Mathiesen, "Large combined heat and power plants in sustainable energy systems," *Applied Energy*, vol. 142, pp. 389-395, Mar. 2015.

[5] M. Geidl, "Integrated Modeling and Optimization of Multi-Carrier Energy Systems," Diss. ETH 17141, Eidgenössische Technische Hochschule Zürich, Zürich, 2007.

[6] C. Liu, M. Shahidehpour and Y. Fu, *et al*., "Security-Constrained Unit Commitment With Natural Gas Transmission Constraints," *IEEE Trans. Power Syst*., vol. 24, no. 3, pp. 1523-1536, Aug. 2009.

[7] M. Geidl and G. Andersson, "Optimal power flow of multiple energy carriers," *IEEE Trans. Power Syst.*, vol. 22, no. 1, pp. 145–155, Feb. 2007.

[8] J. Qiu, H. Yang and Z. Dong, *et al*., "A Linear Programming Approach to Expansion Co-Planning in Gas and Electricity Markets," *IEEE Trans. Power Syst.*, vol. 31, no. 5, pp. 3594-3606, Sep. 2016.

[9] F. Liu, Z. H. Bie, X. Wang., "Day-Ahead Dispatch of Integrated Electricity and Natural Gas System Considering Reserve Scheduling and Renewable

Uncertainties," *IEEE Trans. Sustain. Energy*, vol. 10, no. 2, pp. 646-658, Apr. 2019.
[10] G. Zhou, *et al*., "GPU-Accelerated Batch-ACPF Solution for N-1 Static Security Analysis," *IEEE Trans. Smart Grid*, vol. 8, no. 3, pp. 1406-1416, May 2017.
[11] Y. Xu, *et al*., "DGs for Service Restoration to Critical Loads in a Secondary Network," *IEEE Trans. Smart Grid*, vol. 10, no. 1, pp. 435-447, Jan. 2019.
[12] W. F. Tinney and C. E. Hart, "Power flow solution by Newton's method," *IEEE Trans. Power App. Syst.*, vol. PAS-86, no. 11, pp. 1449–1460, Nov. 1967.
[13] H.D. Chiang, T. Wang and H. Sheng, "A Novel Fast and Flexible Holomorphic Embedding Method for Power Flow Problems," *IEEE Trans. Power Syst.,* vol. 33, no. 3, pp. 2551–2562, May 2018.
[14] S. Rao, Y. Feng and D.J. Tylavsky, *et al*., "The Holomorphic Embedding Method, Applied to the Power-Flow Problem," *IEEE Trans. Power Syst.*, vol. 31, no. 5, pp. 3816–3828, Sep. 2016.
[15] Q. Li, S. An, and T. W. Gedra, "Solving natural gas loadflow problems using electric load flow techniques," in *Proc. North Amer. Power Symp*., 2003.
[16] M. Pirouti, "Modelling and analysis of a district heating network," Ph.D. dissertation, School Eng., Cardiff Univ., Cardiff, U.K., 2013.
[17] H.R. Massrur, T. Niknam and J. Aghaei, *et al*., "Fast Decomposed Energy Flow in Large-Scale Integrated Electricity-Gas-Heat Energy Systems," *IEEE Trans. Sustain. Energy*, vol. 9, no. 4, pp. 1565–1577, Oct. 2018.
[18] A. Martinez-Mares and C.R. Fuerte-Esquivel, "A Unified Gas and Power Flow Analysis in Natural Gas and Electricity Coupled Networks," *IEEE Trans. Power Syst.*, vol. 27, no. 4, pp. 2156–2166, Nov. 2012.
[19] X. Liu, N. Jenkins and J. Wu, *et al*. "Combined Analysis of Electricity and Heat Networks," *Energy Procedia*, vol. 61, pp. 155–159, 2014.
[20] A. Shabanpour-Haghighi, A.R. Seifi, "An Integrated Steady-State Operation Assessment of Electrical, Natural Gas, and District Heating Network," *IEEE Trans. Power Syst.*, vol. 31, no. 5, pp. 3636–3647, Sep. 2016.
[21] X. Liu and P. Mancarella, "Modelling, assessment and Sankey diagrams of integrated electricity-heat-gas networks in multi-vector district energy systems," *Applied Energy*, vol. 167, pp. 336–352, Sep. 2016.
[22] J. Shi, L. Wang and Y. Wang, *et al*., "Generalized energy flow analysis considering electricity gas and heat subsystems in local-area energy systems integration," *Energies*, vol. 10, no. 4, pp. 514, Apr. 2017.
[23] Y. Wen, X. Qu and W. Li, *et al*., "Synergistic Operation of Electricity and Natural Gas Networks via ADMM," *IEEE Trans. Smart Grid*, vol. 9, no. 5, pp. 4555–4565, Sep. 2017.
[24] H. Rudnick, L. Barroso, G. Cunha, and S. Mocarquer, "A natural fit: Electricity-gas integration challenges in South America," *IEEE Power Energy Mag*., vol. 12, no. 6, pp. 29–39, Nov./Dec. 2014.
[25] F. Mohammadi, G.A. Nazri, M. Saif, "A Bidirectional Power Charging Control Strategy for Plug-in Hybrid Electric Vehicles," *Sustainability*, vol. 11, no. 16, pp. 4317–4341, Aug. 2019.
[26] F. Mohammadi, "Power Management Strategy in Multi-Terminal VSC-HVDC System," 4th National Conference on Applied Research in Electrical, Mechanical Computer and IT Engineering, pp. 381-396, Oct. 2018.
[27] T. Savola and I. Keppo, "Off-design simulation and mathematical modeling of small-scale CHP plants at part loads", *Appl. Therm. Eng.*, vol. 25, no. 8, pp. 1219-1232, 2005.
[28] M. Geidl, G. Koeppel, P. Favre-Perrod, B. Klockl, G. Andersson, and K. Frohlich, "Energy hubs for the future," *IEEE Power Energy Mag*., vol. 5, no. 1, pp. 24–30, Jan.–Feb. 2007.
[29] "The standard IEEE 14-bus test system," [Online]. Available: http://www.ee.washington.edu/research/pstca/
[30] Bakhouya D.D. Wolf, "Solving gas transmission problems by taking compressors into account," http://www-heb.univ-littoral.fr/dewolf, Sep. 2008.

Gang Zhang (S'18) received the B.Sc. degree in electrical engineering in 2016 from Shandong University, Jinan, China, where he is currently working toward the Ph.D. degree in electrical engineering. His research interests include multi-energy system, power system resilience, distribution system planning, and power system optimization.

Feng Zhang (M'11) received his Ph.D. degree from Shandong University, China, in 2011. He is currently with School of Electrical Engineering, Shandong University, Jinan, China. During 2015 and 2016, he was a Research Associate at Department of Electrical Engineering, The Hong Kong Polytechnic University. In 2017, he was a visiting scholar at the School of Electrical and Information Engineering, The University of Sydney, Sydney, NSW, Australia. His research interests include renewable energy and energy storage.

Ke Meng (M'10, SM'19) received the Ph.D. degree in electrical engineering from the University of Queensland, Brisbane, QLD, Australia, in 2009. He is currently a Senior Lecturer with the School of Electrical Engineering and Telecommunications, The University of New South Wales, Sydney, NSW, Australia. He was previously a Lecturer with the School of Electrical and Information Engineering, The University of Sydney, Sydney, NSW, Australia. His research interests include pattern recognition, power system stability analysis, and wind power and energy storage.

Xin Zhang (M'16, SM'19) received the B.Eng. degree in automation from Shandong University, China, in 2006; the M.Sc. and Ph.D. degrees in electrical power engineering from The University of Manchester, U.K., in 2007 and 2010 respectively.
He is an Associate Professor (Senior Lecturer) in energy systems at Cranfield University, U.K. He was a Power System Engineer in the Electricity National Control Centre at the National Grid, U.K. His research and industrial experience include power system planning and operation, renewable energy integration, and multi-energy systems. He is a Chartered Engineer with the U.K. Engineering Council.

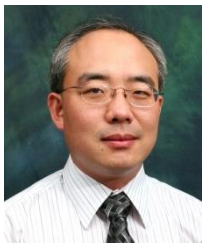

Zhao Yang Dong (M'99–SM'06–F'17) received the Ph.D. degree from the University of Sydney, Sydney, Australia, in 1999. He is currently the SHARP Professor with the University of New South Wales, the Director of ARC Research Hub for Integrated Energy Storage Solutions, and the Director of UNSW Digital Grid Futures Institute, Sydney, NSW, Australia. He was previously a Professor and the Head of the School of Electrical and Information Engineering, The University of Sydney, and the Ausgrid Chair and the Director of the Centre for Intelligent Electricity Networks, University of Newcastle, Callaghan, NSW, Australia. He also held industrial positions with Transend Networks (now TAS Networks), Australia. His research interests include smart grid, power system planning, power system security, load modeling, electricity market, and computational intelligence and its application in power engineering. He is an Editor for the IEEE TRANSACTIONS ON SMART GRID, IEEE TRANSACTIONS ON SUSTAINABLE ENERGY, IEEE POWER ENGINEERING LETTERS, and *IET Renewable Power Generation*.